Supplement of Geosci. Model Dev., 18, 1445–1461, 2025
https://doi.org/10.5194/gmd-18-1445-2025-supplement

Geoscientific Model Development
Open Access

Supplement of

CitcomSVE-3.0: a three-dimensional finite-element software package for modeling load-induced deformation and glacial isostatic adjustment for an Earth with a viscoelastic and compressible mantle

Tao Yuan et al.

Correspondence to: Tao Yuan (tao.yuan@colorado.edu) and Shijie Zhong (shijie.zhong@colorado.edu)

Supplementary Materials

Supplementary Text 1. Pre-calculated ocean function $O(t)$ for first outer iteration

As discussed in section 2.3, a pre-calculated ocean function accounting for the load/ocean transition is used for the first outer iteration in our SLE solver to make the solutions from the first outer iteration as good as possible. The goal is to make it possible to obtain accurate RSL results by running just one forward GIA calculation instead of 3-4 outer iterations, at least under some circumstances. It should be mentioned that the outer iterations are necessary if the initial topography used in the first outer iteration is not ideal, although in our case the present-day topography is a good approximation to the initial topography at the last interglacial period.

Here we describe our approach to derive the pre-calculated ocean function $O(\theta,\phi,t)$ for the first outer iteration. The idea is calculating the change of ocean area (i.e., ocean-continent transitions) based on ice volume change (i.e., $\Delta I(t_i)$) and the present-day topography $T_0(\theta,\phi)$, assuming barystatic sea level change on a rigid Earth (i.e., no radial surface displacement). Note by assuming barystatic sea level change, we mean the total ocean water volume change causes a uniform sea level change globally, which caused the change of ocean area. First, it is easy to find ocean function if the barystatic sea level is known as H (meters higher than the present-day sea level), that is, $O(\theta,\phi,H)=1$ if $T_0(\theta,\phi)-H>0$, and $O(\theta,\phi,H)=0$ otherwise. Then, the barystatic sea level at time t_i can be determined from ice volume change $\Delta I(t_i)$. Define the ocean area $\mathrm{A}(H)=\int_\Omega O(\theta,\phi,H)ds$, where Ω is the surface. By mass conservation, $\int_0^H \rho_w A(h)dh=-\rho_{ice}\Delta I(t_i)$, then, the barystatic sea level H can be determined at stage t_i. Since the $O(\theta,\phi,H)$ is known, the $O(\theta,\phi,t_i)$ is thus determined for each stage t_i.

Supplementary Text 2. A one-iteration solution method for the sea level equation.

For our GIA benchmark with ICE-6G_D, we implemented the multiple outer iteration algorithm by Kendall et al., (2005) for the sea level equation in our semi-analytical code (A et al., 2013). For ICE-6G and VM5a, calculation K3 represents the reference case with convergent solutions after three outer iterations, based on Kendall's original approach. The normalized ocean area which is a measure of the ocean function $O(t)$ for K3 varies between ~0.66 at the last glacial maximum (LGM) and ~0.71 at 122 kybp and the present-day (Fig. S1). Figure S1 also shows the ocean area after the first outer iteration for calculation K3, which, denoted as K1, differs significantly from that of K3. Calculation AS1 represents a single outer iteration model run using our pre-calculated ocean function $O(t)$ as discussed in section 2.3, and AS2 represents the results from the second outer iteration after AS1 using the updated ocean functions $O(t)$ and initial topography T_0, Figure S1 clearly demonstrates that AS1, different from K1, is very similar to K3 and AS2, while the latter two are identical, indicating that the ocean function $O(t)$ for our first outer iteration (AS1) is a fairly accurate representation of the convergent solutions of the Kendall's original approach (K3). Note that the present-day topography is used as initial topography T_0 for calculations AS1 and K1. As discussed below, the reliability of solution from AS1 depends on the differences between the true initial topography and the assumed one (i.e., present-day topography as used here). If there is significant difference between the assumed and true initial topography, updating initial topography is necessary. In our case, the initial stage is the last interglacial period which has similar ice volume to the present day, so the present-day topography is a good approximation to the initial topography.

Using RSL from K3 as standard results, Fig. S2 shows that the maps of RSL difference (i.e., the accuracy) to K3 from calculations AS1, K1 and AS2 at 5 kybp, 10 kybp and 15 kybp. The absolute error in RSL from AS1 is negligibly small for most regions (Fig. S2a, S2d and S2g), whereas the absolute error from K1 is much worse, especially at 20 kybp

(Fig. S2h). AS2 is identical to K3, the standard results (Fig. S2c, S2f and S2i). Admittedly, there are relatively large errors in some localized regions for AS1, such as Hudson Bay and the Arctic Ocean near Fennoscandia for some periods (Fig. S2a and S2d), because we ignore the change in surface radial displacement when deriving the pre-calculated ocean function used in AS1. However, the largest errors in those areas mostly occur in the ocean, while along the coastlines where paleo-relative sea level records are available, the absolute errors are all less than 10 meters (Fig. S2a and S2d). Figure S3 shows the modeled RSL curves at four representative sites including Hudson Bay and Fennoscandia from K3, K1, AS1 and AS2 calculations. The results are consistent with that from Figure S2 in that the errors in modeled RSL from AS1 (i.e., the single outer iteration model run using our revised method for ocean functions) are negligible, whereas the errors from K1 are evident, especially for far-field sites. Note that even at Churchill, which is on the coastline of Hudson Bay, AS1 has negligible errors in RSL calculations.

To further assess the errors in RSL from our AS1 model, we tested two additional GIA calculations with extremely strong or weak mantle viscosity models. For both cases, the lithospheric thickness is 100 km. For the strong mantle case, the entire mantle below the lithosphere has a viscosity of 5×10^{22} Pas. For the weak mantle case, the 200 km thick asthenosphere below the lithosphere and the rest of the mantle have viscosities of 5×10^{18} Pas and 10^{20} Pas, respectively. Figure S4 shows similarly small errors for both cases to that of VM5a (Fig. S2), indicating the reliability of our AS1 model.

Other pre-calculated ocean functions $O(t)$ for any given ice model may be constructed to obtain more accurate RSL results in our AS1 method by replacing the "rigid Earth" approximation with others, for example, the isostasy approximation in which surface elevation changes to compensate the surface loads. Another possible way is to perform a full GIA modeling with three outer iterations (i.e., for outer iterations to converge) for a reference viscosity model and use the ocean functions from the last outer iteration as the pre-calculated ocean functions for any other GIA calculations with reasonable viscosity models in our AS1 method. We test such a strategy by using a reference viscosity model which has a 100-km thick elastic lithosphere and its underlying mantle with a uniform viscosity of 10^{21} Pas and then applying the resulting pre-calculated ocean functions for those same two GIA cases with extremely strong or weak viscosity models as in Figure S4. The resulting errors in RSL for those two cases (Fig. S5) are similar to that in Figure S4 for which the "rigid Earth" approximation was used in building the pre-calculated ocean functions.

To quantify the upper bound of errors in RSL by using one outer iteration (e.g., our AS1 method), we compute 806 GIA models covering a wide range of mantle viscosities and determine RSL histories for a large number of sites in three regions including North America, Fennoscandia, and far fields using both AS1 and K3 methods. The numbers of sites are 18, 12, and 36 for North America, Fennoscandia, and far fields, respectively. The North American and Fennoscandian sites are from Peltier et al., (2015), and the far-field sites are from Lambeck et al., (2014). These models, same as those in Kang et al., (2024), have three viscosity layers: a lithosphere of 100 km thick, the upper and lower mantles, and use ICE-6G_D as the ice history (Peltier et al., 2015, 2018). The viscosity varies from 10^{19} Pas to $10^{21.5}$ Pas in the upper mantle and from $10^{20.5}$ Pas to $10^{23.5}$ Pas in the lower mantle. The relative error (i.e., the relative difference from the reference case K3) in modeled RSL for each site is defined as $\epsilon_i = \frac{\int_0^T |RSL_{x,i}(t) - RSL_{K3,i}(t)| dt}{\int_0^T |RSL_{K3,i}(t)| dt}$, where $RSL_{x,i}$ is the modeled RSL at site i for case K1, AS1, or AS2, $RSL_{K3,i}$ is for the reference case K3, and the integral is for the total model time duration. The regionally averaged relative error ϵ is defined as the average error among all sites within each region, i.e., $\epsilon = \frac{\Sigma \epsilon_i}{N}$, where N is the total number of sites within each region. The maximum regionally averaged relative error among those 806 GIA models is less than 5% (Supplement Table 2) for our AS1 method.

We also quantify the maximum absolute error in RSL, defined as the maximum of $|RSL_x(t) - RSL_{K3}(t)|$ among all time periods t and all sites in each region from those 806 calculations (Supplement Table 2). For far-field sites where RSL is mainly controlled by ocean functions and ice volume changes, the maximum absolute error in RSL is less than 3 meters for the AS1 method but more than 10 meters for the K1 method, consistent with Fig. S1 in that AS1 provides more accurate ocean functions than K1. However, the maximum absolute error in near-field RSL is more significant and up to ~23 meters for both AS1 and K1 methods, reflecting the fact that near-field ocean functions and paleo-topography are more affected by visco-elastic deformation. Fig. S6 shows the RSL curves for the site and viscosity model corresponding to the maximum absolute error of ~23 meters in RSL for AS1. Note that at the site for this case with the maximum absolute error, the total RSL change exceeds 600 meters and the RSL from AS1 is not significantly different from that from K3 (Fig. S6). Depending on factors including the user's goal, RSL data quality, and requirements for accuracy and efficiency of GIA calculations, AS1 could be a viable method to obtain reliable RSL in both far fields and near fields with minimal computational cost.

We summarize our attempts to get accurate RSL results from a single complete GIA model run as follows. Since the purpose of multiple outer iterations is to update ocean function history and initial topography successively to be consistent with the present-day topography and a given ice model (Kendall et al., 2005), our strategy is to construct pre-calculated ocean functions and initial topography that would lead to RSL solutions with an adequate level of accuracy with a single complete GIA model run (i.e., the AS1 method). The present-day topography would be a good approximation for initial topography if a model starts with an ice-sheet distribution similar to that of the present day (i.e., the interglacial period), as in the benchmark study here. We found that three outer iterations of complete model runs with successively updated ocean functions and initial topography could be replaced with our AS1 method, depending on users' goals and requirements for the error levels. For example, studies on global properties of RSL could achieve adequately accurate results from one single complete run (i.e., AS1) with properly constructed pre-calculated ocean functions, as we discussed. If the goal is to model the RSL for one particular near-field site as accurately as possible, it would be more prudent to run two or three outer iterations of complete GIA runs with successively updated ocean functions and initial topography following Kendall et al. (2005). It is worthwhile to mention that, when modeling RSL changes, one should also consider other factors including the errors in RSL records (often exceeding 10 m in near field during the rapid deglaciation (Peltier et al., 2015; Lambeck et al., 2017)), the relatively low resolution of global ice models, inherent numerical errors, and unaccounted processes in the current sea level equation (e.g., erosion and sedimentation).

Supplement Table 1: Comparison of Load Love Numbers h_l, k_l, and l_l Between CitcomSVE and Semi-Analytical Solutions and the corresponding errors.

case	h(0)	k(0)	$\lvert l(0)\rvert$	h(40)	k(40)	$\lvert l(40)\rvert$	ε_{ha}	ε_{ka}	ε_{la}	ε_{hd}	ε_{kd}
Analytic_l1	-1.2543	-1.0000	0.8866	-1.4964	-1.0000	1.9090					
l1m0_R1	-1.2527	-1.0000	0.8869	-1.4943	-1.0000	1.9171	1.37E-03	2.00E-06	2.67E-03	3.99E-04	5.56E-05
l1m0_R2	-1.2548	-1.0000	0.8859	-1.4967	-1.0000	1.9115	2.29E-04	1.00E-06	8.68E-04	1.01E-04	1.50E-05
l1m0_R3	-1.2547	-1.0000	0.8846	-1.4968	-1.0000	1.9105	2.66E-04	0.00E+00	5.10E-04	4.39E-05	6.58E-06
l1m0_R4	-1.2546	-1.0000	0.8864	-1.4968	-1.0000	1.9101	2.91E-04	0.00E+00	4.00E-04	2.50E-05	3.94E-06
Analytic_l2	-0.9577	-0.3041	0.0200	-2.4066	-0.9396	0.8216					
l2m0_R1	-0.9549	-0.3037	0.0201	-2.4000	-0.9373	0.8305	2.43E-03	1.91E-03	7.19E-03	3.64E-04	4.13E-04
l2m0_R2	-0.9578	-0.3039	0.0202	-2.4060	-0.9388	0.8242	1.24E-04	4.98E-04	2.19E-03	9.54E-05	1.04E-04
l2m0_R3	-0.9585	-0.3042	0.0200	-2.4064	-0.9391	0.8232	1.79E-04	2.51E-04	1.38E-03	4.25E-05	4.61E-05
l2m0_R4	-0.9574	-0.3038	0.0203	-2.4066	-0.9392	0.8229	2.30E-04	1.85E-04	1.10E-03	2.30E-05	2.65E-05
Analytic_l2m1	-0.3058	1.0944	0.1118	0.6151	2.1973	0.1884					
l2m1_R1	-0.3094	1.0836	0.1103	0.5583	2.1294	0.1653	7.10E-02	2.08E-02	8.97E-02	8.10E-03	5.82E-04
l2m1_R2	-0.3063	1.0925	0.1116	0.6077	2.1885	0.1847	1.01E-02	2.89E-03	1.46E-02	1.07E-03	6.46E-05
l2m1_R3	-0.3100	1.0900	0.1111	0.6144	2.1964	0.1878	1.78E-03	4.93E-04	3.08E-03	8.14E-04	6.37E-05
l2m1_R4	-0.3056	1.0948	0.1118	0.6178	2.2003	0.1891	2.99E-03	7.52E-04	2.34E-03	4.99E-04	3.60E-05
Analytic_l4	-1.0251	-0.1342	0.0568	-4.4402	-0.9416	0.3411					
l4m0_R1	-1.0194	-0.1341	0.0565	-4.4105	-0.9339	0.3480	6.18E-03	7.58E-03	1.25E-02	3.70E-04	1.42E-03
l4m0_R2	-1.0254	-0.1343	0.0569	-4.4354	-0.9397	0.3432	9.21E-04	1.94E-03	3.60E-03	9.21E-05	3.58E-04
l4m0_R3	-1.0253	-0.1342	0.0569	-4.4384	-0.9407	0.3425	3.29E-04	9.63E-04	2.29E-03	4.22E-05	1.58E-04
l4m0_R4	-1.0247	-0.1341	0.0569	-4.4395	-0.9410	0.3423	1.25E-04	6.08E-04	1.89E-03	2.39E-05	9.24E-05
Analytic_l8	-1.2376	-0.0772	0.0302	-8.8405	-0.9605	0.0958					
l8m4_R1	-1.2172	-0.0767	0.0301	-8.5145	-0.9171	0.1048	3.09E-02	3.94E-02	3.54E-02	6.22E-04	4.94E-03
l8m4_R2	-1.2354	-0.0772	0.0302	-8.7607	-0.9492	0.0980	7.26E-03	1.01E-02	8.95E-03	1.60E-04	1.21E-03
l8m4_R3	-1.2359	-0.0771	0.0304	-8.7960	-0.9544	0.0977	3.85E-03	5.29E-03	8.55E-03	7.12E-05	5.91E-04
l8m4_R4	-1.2372	-0.0772	0.0303	-8.8084	-0.9563	0.0977	2.63E-03	3.56E-03	8.50E-03	4.21E-05	3.02E-04
Analytic_l16	-1.6868	-0.0574	0.0229	-17.8470	-0.9726	0.0479					
l16m8_R1	-1.5913	-0.0544	0.0225	-15.0636	-0.7883	0.0329	1.39E-01	1.74E-01	2.55E-01	1.00E-03	2.05E-02
l16m8_R2	-1.6660	-0.0568	0.0228	-17.0264	-0.9179	0.0418	3.88E-02	4.92E-02	9.26E-02	2.52E-04	4.86E-03
l16m8_R3	-1.6781	-0.0572	0.0228	-17.3994	-0.9437	0.0430	2.06E-02	2.54E-02	7.45E-02	1.12E-04	2.14E-03
l16m8_R4	-1.6825	-0.0573	0.0228	-17.5347	-0.9530	0.0435	1.40E-02	1.69E-02	6.71E-02	6.60E-05	1.20E-03
l16m8_R5	-1.6805	-0.0572	0.0228	-17.6230	-0.9579	0.0464	1.04E-02	1.31E-02	2.26E-02	6.50E-05	1.33E-03

ε_{ha}, ε_{ka}, and ε_{la} are amplitude errors for Love numbers h, k, and l, respectively. ε_{hd} and ε_{kd} are dispersion errors for Love numbers h and k, respectively.

Supplement Table 2: Maximum errors in modeled RSL from different cases compared to the reference case (K3) among an ensemble of semi-analytical calculations with a wide range of viscosity models

	North America[a]	Fennoscandia	Far Field
K1[c]	6.54% (22.8 m)[b]	4.81% (10.0 m)	4.69% (10.6 m)
AS1	4.53% (23.2 m)	4.89% (11.0 m)	2.97% (2.7 m)
AS2	0.49% (4.5 m)	0.32% (0.8 m)	0.19% (0.4 m)

a. "North America", "Fennoscandia", and "Far Field" are regions with groups of sites used in calculating RSL. The numbers of sites are 18, 12, and 36 for North America, Fennoscandia, and Far Field, respectively. The North American and Fennoscandian sites are from (Peltier et al., 2015). The far-field sites are from (Lambeck et al., 2014).

b. The relative error in modeled RSL for each site is defined as $\epsilon_i = \frac{\int_0^T |RSL_{x,i}(t) - RSL_{K3,i}(t)|dt}{\int_0^T |RSL_{K3,i}(t)|dt}$, where $RSL_{x,i}$ is modeled RSL at site i for case K1, AS1, or AS2, and $RSL_{K3,i}$ is for the reference case K3. The regionally averaged relative error is defined as the average error among all sites within each region, i.e.,$\frac{\Sigma\epsilon_i}{N}$, where ϵ_i is the error for each site i and N is the total number of sites within each region. The numbers out of parenthesis represent the maximum region-averaged relative error among the 806 calculations of varying mantle viscosity. The numbers inside parenthesis represent the maximum absolute error (i.e., $\max(|RSL_x(t) - RSL_{K3}(t)|)$) among all time periods t and all sites in each region from those 806 calculations of varying mantle viscosity. Those numbers measure the maximum possible error for each case among reasonable mantle viscosity structures.

c. The meaning of case K1, AS1, and AS2 can be found from the main text.

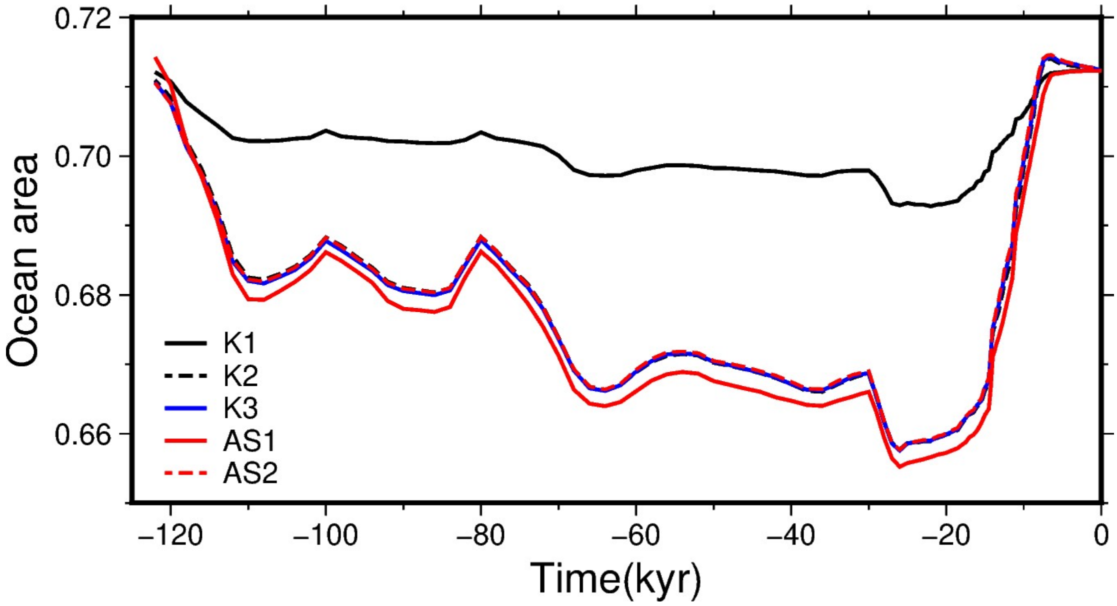

Figure S1. Normalized ocean areas determined from the ocean functions from five different semi-analytical calculations: K1, K2, K3, AS1, and AS2.). Calculation K3, the reference case, represents the convergent solutions after the third outer iteration based on the algorithm from Kendall et al., (2005), while K1 is that after the first outer iteration and K2 is the after the second outer iteration. AS1 represents the first outer iteration based on the pre-calculated ocean functions determined assuming rigid Earth, and AS2 is the second outer iteration with updated ocean functions and initial topography following AS1. Note that K2, K3 and AS2 are almost overlapping with each other.

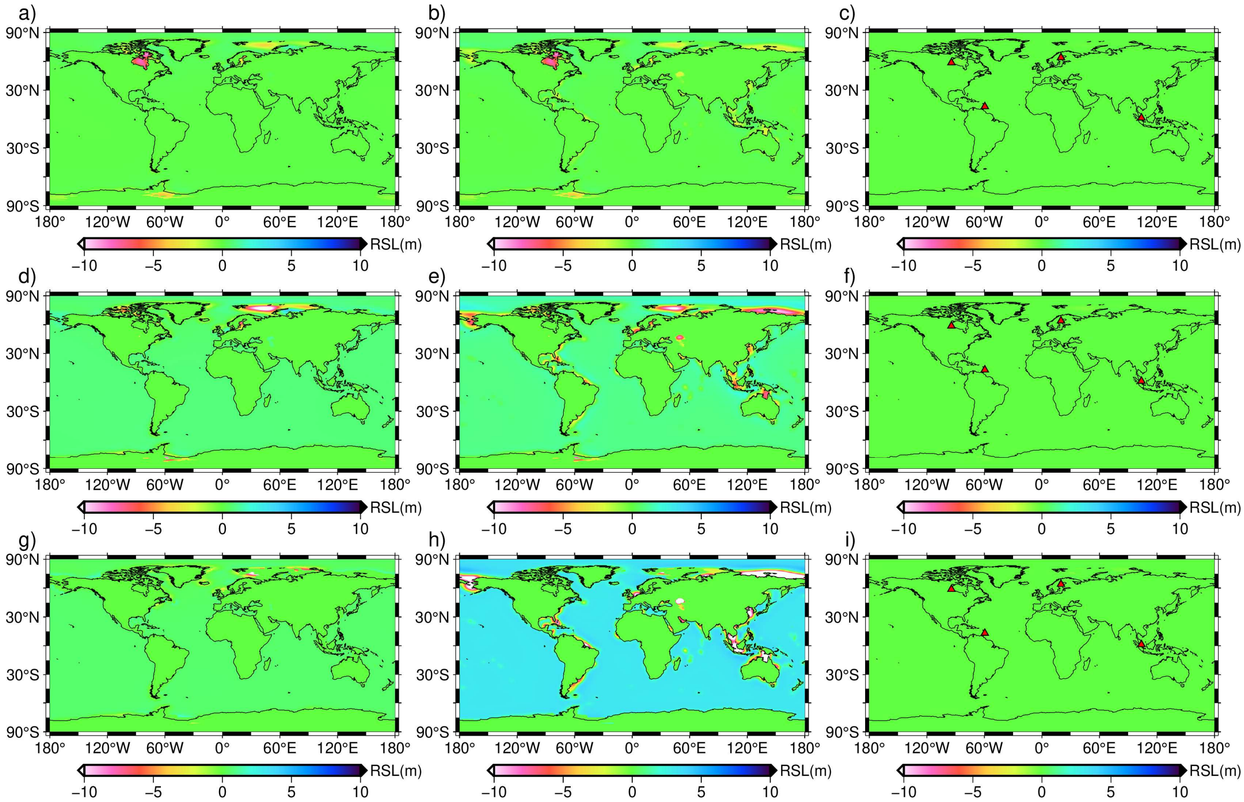

Figure S2. Comparison of modeled relative sea level (RSL) at 5 kybp (the top row), 10 kybp (the middle row), and 15 kybp (the bottom row) among four different semi-analytic calculations: K1, K3, AS1 and AS2. Shown here are the differences (or the errors) in RSL to reference case K3 from AS1 (the left column, a, d, and g), K1 (the middle column, b, e and h), and AS2 (the right column, c, f, and i), respectively. The difference (or error) at a given time is defined as $(RSL_x - RSL_{\mathrm{K3}}) \cdot O_x$, where x is AS1, K1, or AS2, O_x is the ocean function. Note that RSL is only meaningful for ocean regions (including coastlines), since RSL records at one site can exist only if this site is ocean for that time period. The red triangles in the last column represent sites in Figure S3. Note the ice model and viscosity model used are ICE6G and VM5a.

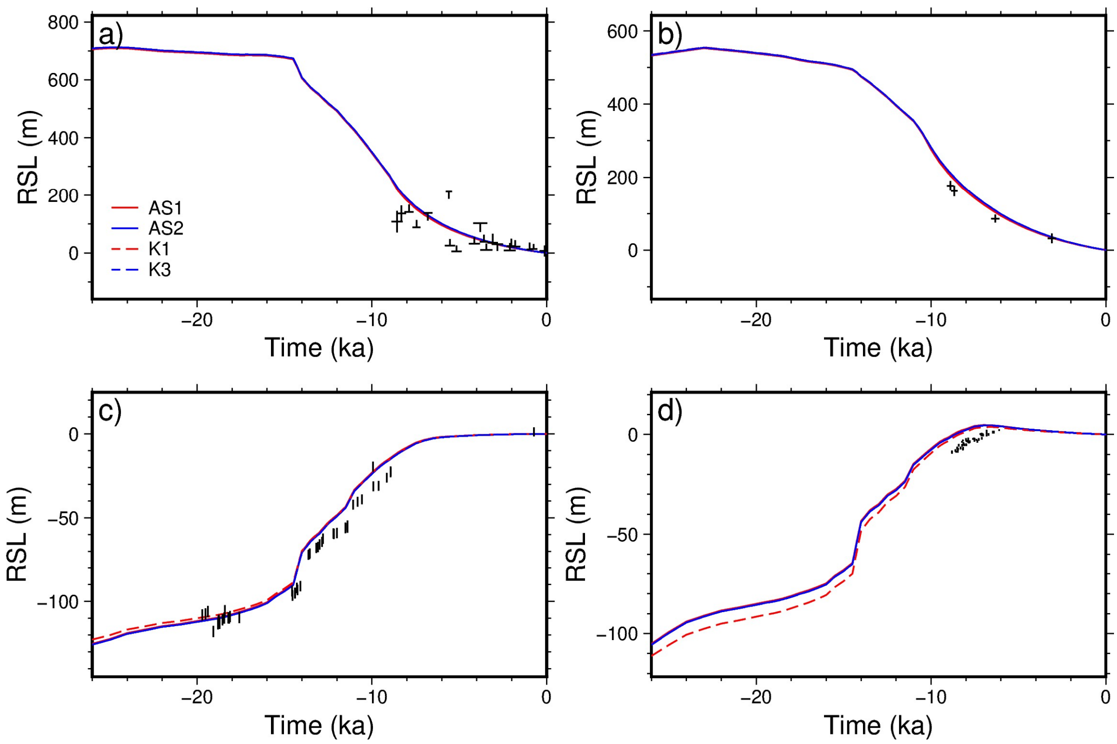

Figure S3. Comparison of modeled RSL curves at four sites from four semi-analytic calculations (AS1, K1, AS2, and K3 as in Figure S1): Churchill (Hudson Bay) (a), Vasterbotten (b), Barbados (c), and Geylang (d) (i.e., same sites as in Figure 6 where their longitudes and latitudes are given). The locations of those four sites are also shown in Figure S2.

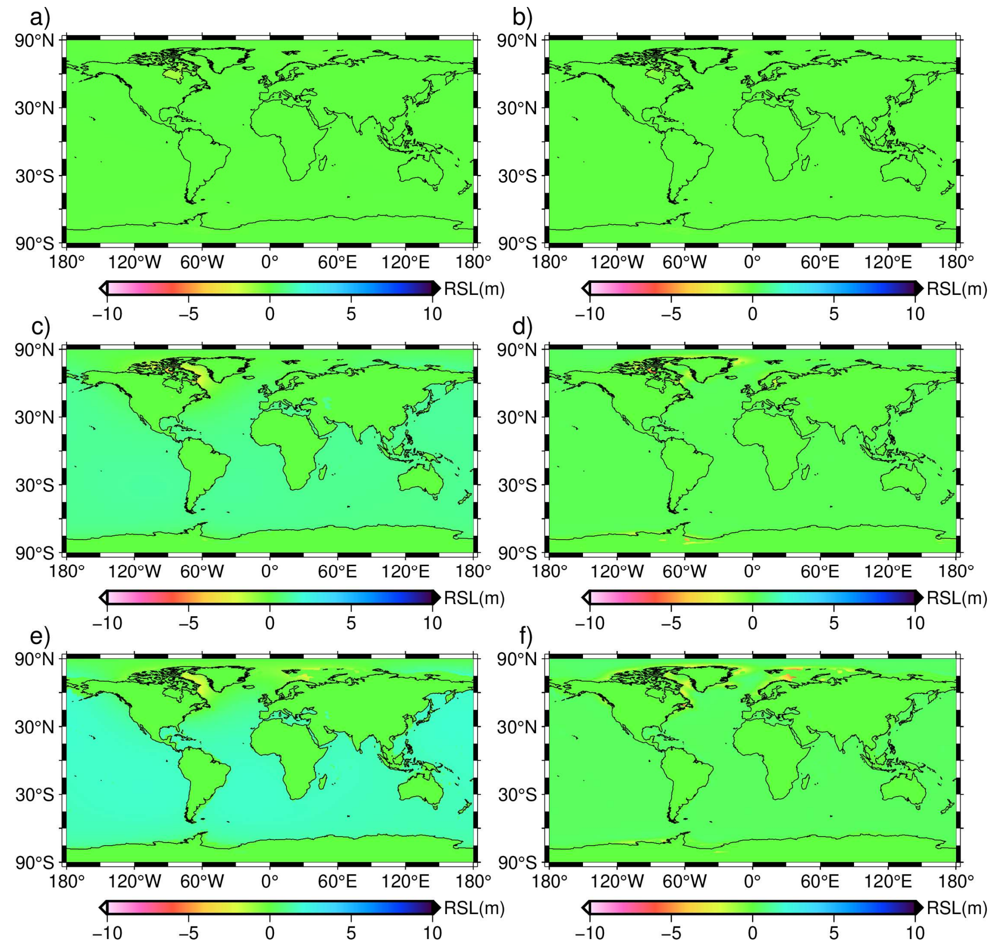

Figure S4. The RSL differences to calculation K3 from calculation AS1, or $(RSL_{AS1} - RSL_{\mathrm{K3}}) \cdot O_{AS1}$, for the case with an extremely strong mantle (the left column, a, c, and e for 5 kybp, 10 kybp and 15 kybp, respectively), and the case with an extremely weak mantle (the right column, b, d, and f for 5 kybp, 10 kybp and 15 kybp, respectively). Note that the pre-calculated ocean functions for both cases are constructed assuming a "rigid Earth".

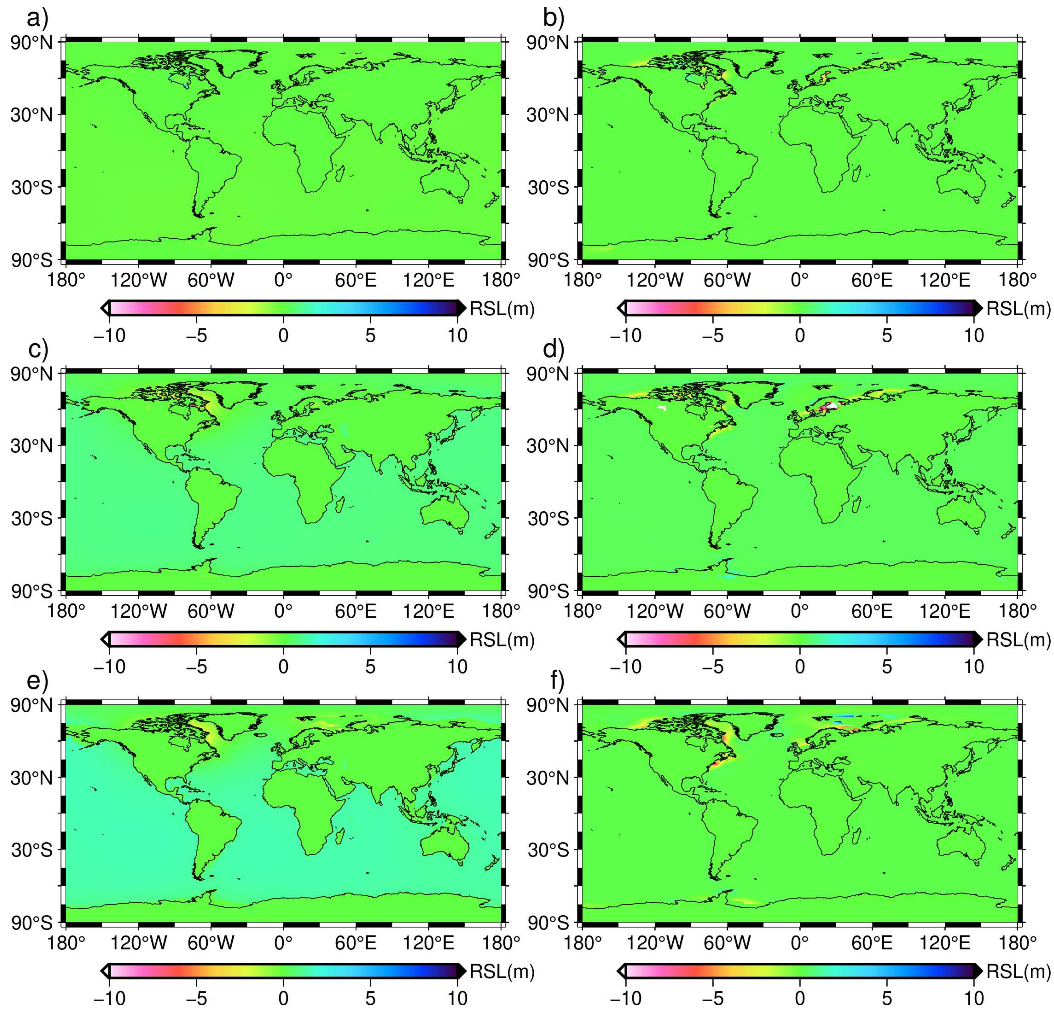

Figure S5. The same as in Figure S4, except for using different pre-calculated ocean functions. The RSL differences to calculation K3 from calculation AS1, or $(RSL_{AS1} - RSL_{\mathrm{K3}}) \cdot O_{AS1}$, for the case with an extremely strong mantle (the left column, a, c, and e for 5 kybp, 10 kybp and 15 kybp, respectively), and the case with an extremely weak mantle (the right column, b, d, and f for 5 kybp, 10 kybp and 15 kybp, respectively). The pre-calculated ocean functions for both cases are constructed from the convergent solutions (i.e., with three outer iterations) using Kendall et al., (2005) for a reference viscosity model (i.e., 100-km thick lithosphere overlying the mantle with uniform viscosity of 10^{21} Pas). Note that the reference viscosity model is only used for constructing the pre-calculated ocean functions.

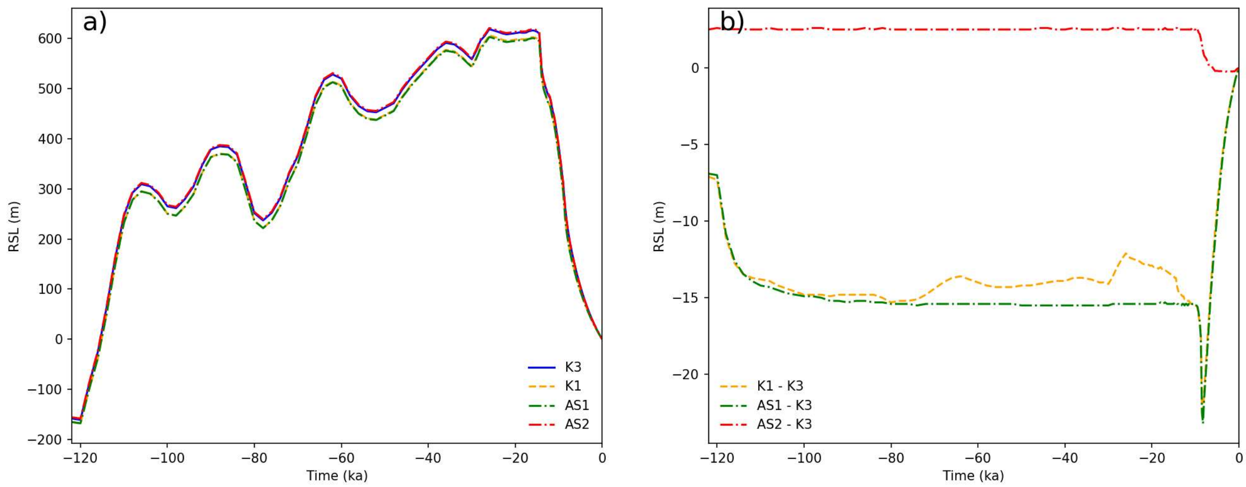

Figure S6. The modeled RSL (a) for calculations for the site and the viscosity model that yields the maximum absolute error presented in Supplement Table 2 (i.e. 23.20 m, the maximum absolute error for AS1 in North America). (b) shows the differences in RSL between K1, AS1, and AS2 to the reference case K3 for that site and viscosity model. The site is Churchill, and the mantle viscosities are 1.26×10^{20} Pas and 1.26×10^{23} Pas for upper and lower mantle, respectively.